Civil Engineering and Applied Solutions

Research Article

journal homepage: ceas.journals.umz.ac.ir

CEAS Civil Engineering and Applied Solutions

Numerical Investigation of Fe-SMA Strengthened Masonry Walls under Lateral Loading

Moein Rezapour [a], Mehdi Ghassemieh [a*]

[a] *College of Engineering, School of Civil Engineering, University of Tehran, Tehran, Iran*

ARTICLE INFO

Keywords:
Masonry wall
Shape memory alloy
Post-tensioning
Iron-based

Article history:
Received 02 July 2025
Accepted 27 July 2025
Available online 01 September 2025

ABSTRACT

This study explores the application of Fe-based shape memory alloys (Fe-SMAs) for the seismic strengthening of unreinforced masonry (URM) walls. Due to their unique thermomechanical behavior and cost-effectiveness, Fe-SMAs offer a promising alternative to traditional reinforcement materials. Using Abaqus finite element software, numerical models were developed and validated against experimental results to examine the structural performance of masonry walls reinforced with Fe-SMA strips. Three reinforcement configurations were investigated: vertical, V-shaped, and Λ-shaped layouts, each subjected to different levels of post-tensioning stress ranging from 100 MPa to 400 MPa. The results revealed a substantial improvement in lateral resistance and stiffness across all models. The vertically reinforced walls exhibited the highest gains, with up to a 96% increase in base shear resistance. V-shaped and Λ-shaped reinforcements also showed significant enhancements, mainly due to the bracing effect of the inclined SMA strips. While the failure mode remained primarily diagonal shear in all cases, the introduction of post-tensioning delayed crack initiation and improved energy dissipation capacity. The frictional interaction between the SMA strips and masonry units, augmented by the post-tensioning force, was identified as a key factor in enhancing performance. This study demonstrates that Fe-SMA reinforcement is a viable, innovative technique for retrofitting masonry walls, especially in earthquake-prone regions. The ease of installation, combined with the ability to apply force through thermal activation, makes Fe-SMAs a highly practical solution for improving the safety and resilience of existing masonry structures.

1. Introduction

Masonry materials are among the oldest building materials used in construction. Their abundance, compatibility with most climatic conditions, lack of need for specialized labor during construction, durability, and long-lasting properties are some of the reasons why these materials have continuously been favored in building projects. A large portion of the buildings worldwide are constructed with masonry materials. However, the understanding and knowledge of structural engineers regarding the behavior of such structures are still insufficient, and further research is necessary to accurately understand the behavior of masonry as a structural material. This need is especially felt in countries located on seismic belts, where residents of masonry buildings have suffered irreparable damage in recent earthquakes. Since a significant portion of the world's population lives in these types of structures, finding methods to enhance the resistance of masonry buildings is extremely important.

Recent earthquakes have tragically demonstrated the vulnerability of unreinforced masonry (URM) buildings. For example, during the 2023 Türkiye–Syria earthquake, more than 50,000 people were killed, and over 200,000 buildings were either destroyed or severely damaged, many of which were URM structures. Similarly, in the 2017 Mexico City earthquake, approximately 60% of the collapsed structures were unreinforced masonry buildings. These catastrophic events underscore the urgent need for reliable

* Corresponding author.
E-mail addresses: m.ghassemieh@ut.ac.ir (M. Ghassemieh).

https://doi.org/10.22080/ceas.2025.29594.1022
ISSN: 3092-7749/
How to cite this article: Rezapour, M., Ghassemieh, M. Numerical Investigation of Fe-SMA Strengthened Masonry Walls under Lateral Loading. Civil Engineering and Applied Solutions. 2025; 1(4): 1–15. doi:10.22080/ceas.2025.29594.1022.

seismic retrofitting techniques. Therefore, developing effective and economical solutions, such as the application of Fe-based Shape Memory Alloys (Fe-SMAs), is crucial to improving the resilience of existing masonry infrastructure in earthquake-prone regions.

Understanding the behavior of masonry structures for their strengthening is an inevitable process. Therefore, many studies have been conducted on these structures. Maheri et al. [1], in their experimental research, they demonstrated that the use of a head mortar can lead to increased shear strength and wall out-of-plane stiffness. Similar results were also observed by Nateghi and Alemi [2], based on the effect of head mortar on wall behavior through laboratory tests. Griffith et al. [3] examined the out-of-plane behavior of masonry walls under lateral loads in their studies. They subjected eight unreinforced masonry walls to cyclic static out-of-plane loading. Their observations showed that increasing axial load resulted in less resistance drop in the wall, and this was consistent across all walls. ElGawady et al. [4] demonstrated, based on their experimental tests, that the type of mortar significantly influences the wall's resistance, crack pattern, and ductility. According to experiments by Gouveia and Lourenço [5], the use of reinforcement mesh for unifying the masonry wall can increase the lateral resistance and ductility of the unreinforced masonry wall by up to 30%. Petry and Beyer [6], in a study aimed at providing necessary data to improve numerical models of unreinforced masonry walls, investigated the effect of boundary conditions on masonry wall behavior. They subjected six unreinforced masonry walls with clay units and cement mortar to cyclic loading. Wang et al. [7] studied the effect of reinforcement mesh on masonry walls with openings. Their findings indicated that openings reduce the confinement effect of the reinforcement mesh; however, using reinforcement results in more continuous and ductile behavior compared to unreinforced walls. ElGawady et al. [8] used FRP strips for the seismic retrofit of an unreinforced masonry wall. They applied the FRP strips in a cross pattern to improve the wall's behavior and observed that while the initial stiffness of the retrofitted wall was similar to that of a regular wall, the failure mode shifted from shear to bending, making the wall more ductile. Shabdin et al. [9] found that walls equipped with concrete overlays exhibit relatively high energy dissipation capacity, and their cyclic behavior shows less buckling effect. Various methods have been introduced for strengthening masonry structures. One of these methods involves increasing the axial load applied to masonry walls. In this approach, the structural resistance of the wall is enhanced by increasing the applied axial load. This increase can be achieved through post-tensioning of the wall [10].

According to Sadeghi Marzaleh [11] research, increasing the axial load on a wall can enhance its shear resistance while reducing its displacement capacity. He also observed that excessive compressive stress induced by post-tensioning might change the failure mode from shear to diagonal cracking. This increase in axial load can be applied to the wall using post-tensioning elements such as steel tendons or rebars. Various methods and materials have been introduced for the post-tensioning of masonry walls. Schultz and Scolforo [12] studied the effect of post-tensioning on the out-of-plane behavior of masonry walls subjected to wind loads. They observed that applying post-tensioning significantly improves the wall's resistance to wind loads perpendicular to its plane. Kohail et al. [13] investigated the effect of post-tensioning on a specific type of masonry shear wall made of concrete blocks. Their research mainly focused on how post-tensioning influences the failure mode, permanent deformation, energy dissipation capacity, stiffness, and ductility of masonry walls. Soltanzadeh et al. [14] examined the effect of post-tensioning on shear walls made of confined masonry. Their studies indicated that masonry walls equipped with confined post-tensioning systems exhibit good ductility. Hassanli conducted extensive research on the performance factors of post-tensioned masonry structures [15-18]. To accurately assess this, he proposed modeling methods aimed at predicting the seismic behavior of these post-tensioned walls. The results showed that the numerical models were reasonably accurate, and using these models, they could derive factors for the performance analysis of post-tensioned masonry walls. Laursen and Ingham [19] conducted a study to establish appropriate seismic design criteria for post-tensioned masonry structures. Most of their research focused on the effects of post-tensioning with unbonded tendons on in-plane behavior. Quiroz [20] studied the seismic performance of four historic masonry towers reinforced with unbonded AFRP tendons. Babatunde [21] tested different reinforcement methods on unreinforced masonry walls. One of these methods, which showed a good response to lateral loads, was post-tensioning the wall using FRP materials. Seim et al. used FRP for localized post-tensioning in masonry materials and demonstrated that applying post-tensioning at points with the highest damage potential can significantly improve the seismic behavior of masonry walls [22].

In this article, shape memory alloys are used for the purpose of wall strengthening in buildings. The proposed alloy is iron-based, which is more economical compared to other alloys. These alloys can generate a significant amount of post-tensioning force through heat absorption. Therefore, many researchers have studied this property of shape memory alloys.

Hong et al. [23] researched evaluating the recovery behavior of iron-based shape memory alloys (Fe-SMA) under various constraints. Choi et al. [24] investigated the effect of prestressing embedded Fe-SMA wires on the flexural behavior of mortar beams. Experimental data indicated that the prestressing force could reduce the resulting stress by approximately 28% in both tensile and compressive parts of the mortar beams. Shahverdi et al. [25-27] examined the feasibility of using a form of Fe-SMA that is economically advantageous for post-tensioning concrete beams. Izadi et al. [28-31] also explored the potential of using the reversibility property of these alloys in metal strips and a steel bridge. Rezapour et al. [32] investigated the potential application of these alloys in structural walls. They modeled the walls at a macroscopic scale and bonded SMA strips to the walls. Based on the results obtained, these alloys significantly increased the energy dissipation capacity of the walls.

Prestressing in structural walls is primarily applied in the vertical direction. Implementing prestressing diagonally in building walls is rarely done due to construction difficulties. Shape memory alloy strips, owing to their unique behavior and simple installation method, enable the possibility of diagonal prestressing of building walls. Therefore, in this study, walls with prestressed materials are examined both in the vertical and diagonal orientations under various load distribution levels. To achieve this, a masonry wall was modeled using Abaqus software, and the results were validated against experimental data. These models incorporated iron-based prestressed strips subjected to both vertical and diagonal prestressing. The results of these analyses, in terms

of performance and failure modes, were compared with each other.

2. Fe-based shaped memory alloys

Fe-based shape memory alloys are innovative materials distinguished by their unique properties among various alloys. These alloys can revert to their original shape upon absorption of a certain amount of heat. To date, various types of shape memory alloys have been discovered and developed. Among these, iron-based alloys constitute a specific category, with the primary element in their atomic structure.

From an economic perspective, these alloys are more cost-effective compared to other shape memory materials and can be utilized in generating residual stresses within civil engineering structures. The process of inducing residual stress in these alloys involves several steps: initially, a significant deformation is applied; this is followed by imposing specific boundary conditions; and finally, the alloy is heated. Upon heating, the alloy tends to regain its original shape; however, the boundary conditions inhibit this transformation. As a result, depending on the extent of the deformation, boundary conditions, and the temperature applied, residual stresses develop within the alloy. This process is illustrated in Fig. 1, which depicts the step-by-step progression.

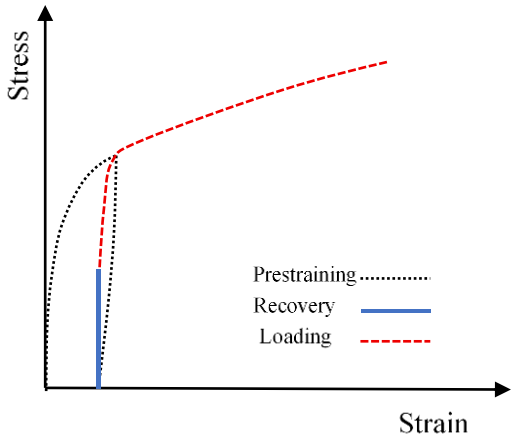

Fig. 1. Stress-strain curve of activated Fe-SMA.

Generally, these materials possess two distinct atomic structures: austenite and martensite (Fig. 2). These structures can be interconverted through the application of temperature and/or stress. The shape memory behavior in Fe-SMAs arises from the stress-induced transition of martensite from the parent γ-austenite phase to the ε-martensite phase at lower temperatures. The reverse transformation, from martensite back to austenite, occurs exclusively at elevated temperatures [33].

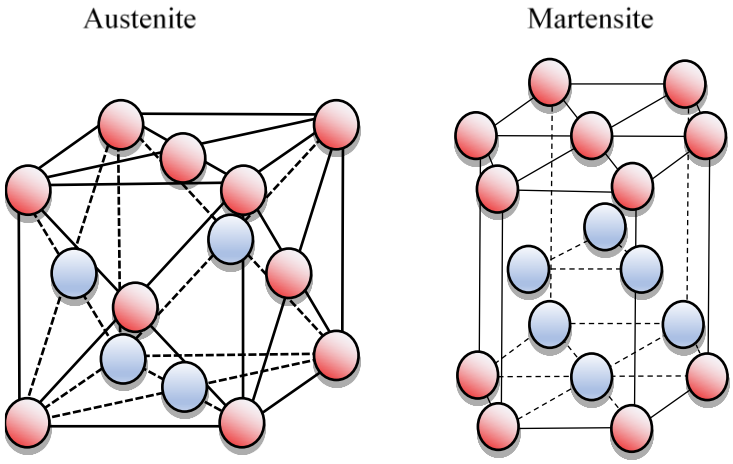

Fig. 2. Phase transformation of the Fe-based SMA.

3. Model description

In this paper, data and results from the experimental studies conducted Vermeltfoort et al. [34] on masonry walls are utilized. In the aforementioned experimental research, the masonry wall was subjected to in-plane lateral loading. The dimensions of the studied wall are 990 mm in length, 1140 mm in height, and 100 mm in thickness. The wall consists of 18 rows of clay bricks, each having a length of 210 mm, a height of 52 mm, and a thickness of 100 mm. The mortar thickness is 10 mm, and the mix ratio of cement, lime, and sand is 1:2:9. In the experimental model, a steel beam and foundation were used. However, since in this study, the masonry wall needs to be reinforced with SMA strips, which are connected to the concrete, an elastic beam and foundation with dimensions of 900×100×100 mm were used instead of the steel beam and foundation. A uniform vertical load of 0.3 MPa is applied at the top of the beam. This load remains constant throughout the loading process and simulates the weight of the upper floor. The lateral load is applied to the masonry wall in a monotonic, in-plane manner (Fig. 3).

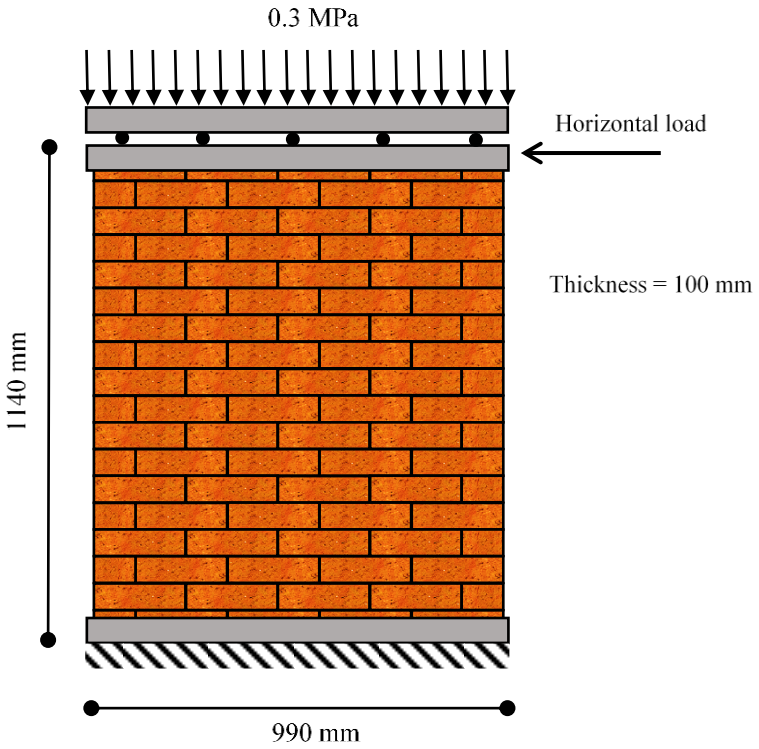

Fig. 3. Geometric characteristics of the masonry wall.

4. Modeling

Modeling of a masonry structure can be performed using three different methods. The first method is called Detailed Micro-modeling (Fig. 4a), which provides the highest level of accuracy. In this approach, the masonry units (bricks) and the mortar between them are fully modeled. Since all the parameters of the masonry wall are considered in this modeling technique, the resulting numerical model has a large stiffness matrix, leading to a significantly long analysis time [35].

The second method is known as Simplified Micro-modeling (Fig. 4b), which has lower accuracy compared to the first method but still maintains an acceptable level of precision. In this approach, the masonry units are modeled larger than their actual size. The increase in size corresponds to the thickness of the mortar joints between the bricks. The mortar is not directly modeled in this method; instead, its mechanical behavior is represented through the interaction between adjacent bricks. By omitting the mortar elements, the size of the stiffness matrix is reduced compared to the first method, which significantly decreases the required analysis time [35].

While both the Detailed Micro-model and Simplified Micro-model approaches are suitable for modeling a single masonry wall, they become very time-consuming when used for modeling an entire masonry structure. In large structures, the Macro-modeling approach is typically used (Fig. 4c). Although this method is less accurate than the other two, it offers much faster analysis times. In Macro-modeling, the entire masonry structure is represented as a homogeneous material similar to concrete. Despite its lower accuracy, this method provides relatively acceptable results when modeling large-scale masonry structures. In general, macro-modeling methods require less computational time compared to other techniques [36].

(a) **(b)** **(c)**

Fig. 4. Modeling of a masonry wall: (a) Detailed micro, (b) Simplified micro, and (c) Macro.

In this study, the effect of post-tensioning on masonry walls is investigated. Since the model involves only a single masonry wall with limited dimensions, the Simplified Micro-modeling method is employed for the numerical modeling of the target masonry wall.

4.1. Modeling of masonry units

As previously mentioned, in the Simplified Micro-modeling approach, the dimensions of masonry units are increased by an amount equal to the thickness of the mortar joints. This expansion eliminates the need to model mortar elements explicitly, and instead, the behavior of the mortar is incorporated into the model through interaction mechanisms assigned between the masonry units.

Since masonry units are brittle materials, the Concrete Damage Plasticity (CDP) model is used to simulate their behavior. The Damage Plasticity Model is based on the hardening and softening behavior of quasi-brittle materials such as concrete and rock masses. It is widely applied in the general analysis of quasi-brittle materials under dynamic or cyclic loading conditions. These types of materials typically exhibit brittle behavior under various loading scenarios. In such cases, the primary failure mechanisms are cracking under tension and crushing under compression [37].

One of the most important features of the CDP model is its ability to distinguish between tensile and compressive yield strengths and to account for stiffness degradation during cyclic and dynamic loading, based on concrete damage parameters. The plasticity model described in this section was initially proposed by Lubliner and later extended by Lee and Fenves. The foundation of this model is based on two main failure mechanisms in concrete: tensile cracking and compressive crushing [37, 38].

In Abaqus software, the Concrete Damage Plasticity (CDP) model is widely employed to simulate damage in concrete structures. This model captures the irreversible degradation of stiffness in brittle materials due to mechanical loading. Stiffness degradation is characterized using two damage parameters: tensile damage (d_t) and compressive damage (d_c).

Fig. 5 illustrates the axial stress–strain behavior of concrete under both tension and compression. In this figure, the material stiffness during loading is reduced by factors of (1−dt) and (1−dc) for tension and compression, respectively. The variables ε_t^{in} and ε_c^{in} represent the inelastic tensile and compressive strains in the undamaged state, while ε_t^{pl} and ε_c^{pl} denote the corresponding plastic strains in the damaged state.

Eqs. 1 and 2 define the relationships between these strain components.

$$\varepsilon_c^{pl} = \varepsilon_c^{in} - \frac{d_c\,\sigma_c}{(1-d_c)E_0} \tag{1}$$

$$\varepsilon_t^{pl} = \varepsilon_t^{ck} - \frac{d_t\,\sigma_t}{(1-d_t)E_0} \tag{2}$$

where, σ_c and σ_t are compressive and tensile stress at any point.

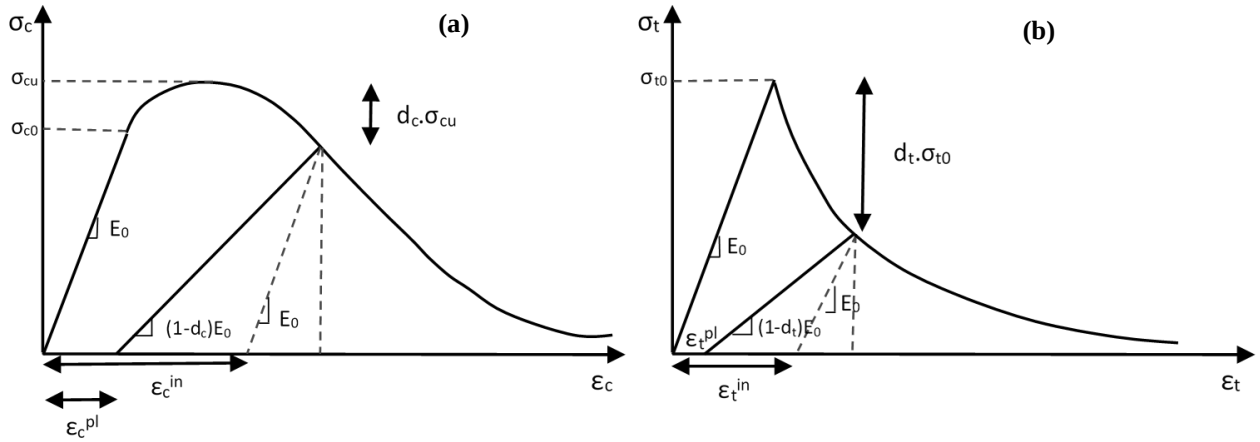

Fig. 5. Stress-strain relationship for CDP model: (a) in compression, and (b) in tension [37].

To simulate the nonlinear behavior of bricks, a constitutive law is required to describe the stress–strain relationship. In this study, it is assumed that the behavior of clay brick is similar to that of low-strength concrete.

The monotonic envelope curve of concrete in compression follows the modified Kent and Park concrete model, which offers good accuracy and simplicity, and has been published by Mander et al. [39]. The formulations of the stress-strain relations of unconfined concrete based on the modified Kent and Park model are summarized here.

The constitutive model consists of an ascending branch represented by a second-degree parabolic curve and a descending linear part. The ascending parabola is expressed by the following equation:

$$f_c = k f'_c \left[\frac{2\varepsilon_c}{\varepsilon_0 k} - \left(\frac{\varepsilon_c}{\varepsilon_0 k}\right)^2\right] \qquad \varepsilon_c \le k\varepsilon_0 \tag{3}$$

where ε_c is the longitudinal concrete strain, f'_c is the compressive strength of concrete. The compression strength of the brick is also assumed to be 15 MPa. ε_0 is the strain of unconfined concrete corresponding to f'_c, and k is a confinement coefficient greater than or equal to 1. Since no confinement is considered for the bricks in the masonry wall modeling, the value of k is assumed to be

equal to one.

For strain greater than the value corresponding to the peak stress, the softening branch of the stress-strain relationship is approximated by a straight line having the equation:

$$f_c = kf'_c[1 - Z_m(\varepsilon_c - \varepsilon_0 k)] \qquad \varepsilon_c > k\varepsilon_0 \tag{4}$$

where Z_m is the strain softening slope and can be calculated by:

$$Z_m = \frac{0.5}{\left[\left(\frac{3 + 0.29f'_c}{145f'_c - 1000}\right) - \varepsilon_0 k\right]} \tag{5}$$

In the tensile regime, the material behavior is simulated using an equation proposed by Selby and Vecchio [40]. According to this equation, the response remains linear up to the peak tensile stress, after which softening behavior occurs in the material.

$$f_t = \frac{f'_t}{1 + \sqrt{200\varepsilon_t}} \qquad \varepsilon_t > \varepsilon_{ct} \tag{6}$$

where ε_t is the longitudinal concrete strain in the tension part, the tensile strength (f'_t) of the brick is also assumed to be 2 MPa. Since the Simplified Micro-modeling approach is used in this study, the dimensions of the masonry units are larger than their actual size. A_s a result, the stiffness of the expanded units differs from that of the original masonry units. To compensate for this discrepancy, the elastic modulus assigned to the expanded units is adjusted and differs from the actual value.

For this purpose, Eq. 7 is proposed based on the assumption of a stack bond between masonry units and uniform stress distribution in masonry constituents. It is presented as:

$$E_{adj} = \frac{HE_uE_m}{nh_uE_m + (n-1)h_mE_u} \tag{7}$$

where H is the height of the masonry assemblage, E_u and E_m are the elastic modulus of unit and mortar, respectively, h_u and h_m are the height of the masonry unit and mortar, and n is the number of courses in a masonry assemblage.

4.2. Mortar modeling

To model the mortar, the surface-based cohesive behavior model is employed. In this approach, the mortar is completely removed from the model, and its mechanical behavior is simulated through interaction definitions. This model consists of both linear and nonlinear regimes and accounts for behavior in three directions: one normal (axial) direction and two shear directions (Fig. 6).

The behavior of the mortar is described using stress–separation relationships, as illustrated in Fig. 7. The shear behavior in the two perpendicular directions is assumed to be approximately similar.

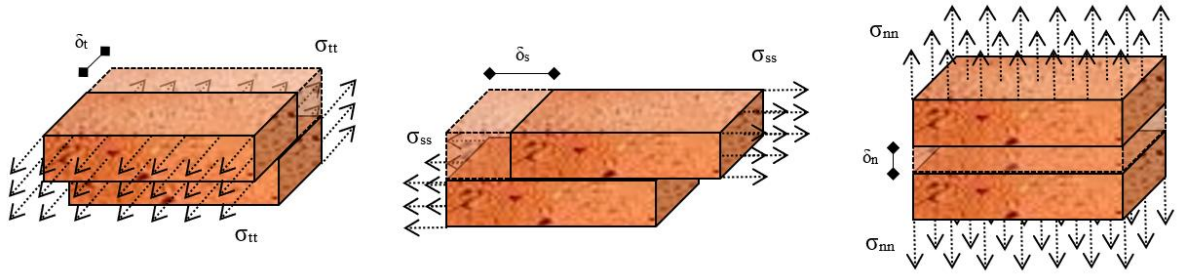

Fig. 6. Linear behavior in interaction: (a) shear in plane, (b) shear perpendicular to the plane, and (c) axial.

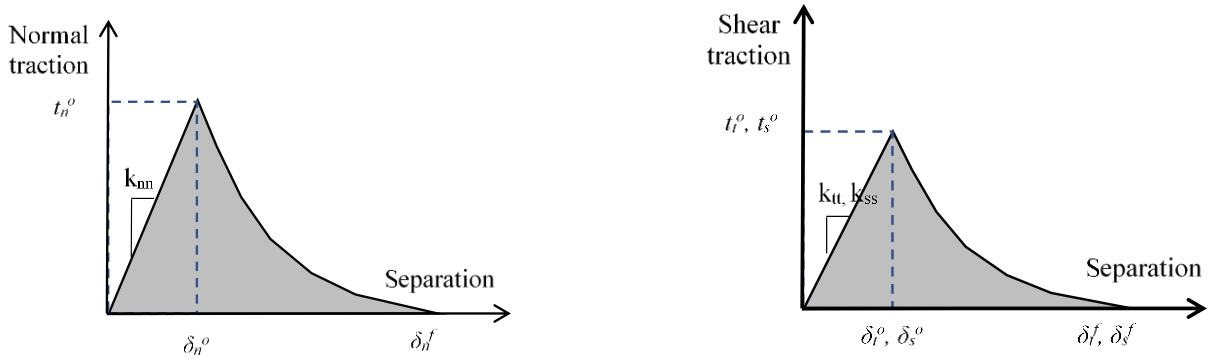

Fig. 7. Nonlinear shear and axial behavior of mortar.

The initial behavior at the joint interfaces is defined as linear stresses based on the amount of relative displacement. This behavior is represented by an elastic stiffness matrix. Eq. 8 presents the relationship between the displacement vector and the stress.

$$\begin{bmatrix} t_n \\ t_s \\ t_t \end{bmatrix} = \begin{bmatrix} k_{nn} & 0 & 0 \\ 0 & k_{ss} & 0 \\ 0 & 0 & k_{tt} \end{bmatrix} \begin{bmatrix} \delta_n \\ \delta_s \\ \delta_t \end{bmatrix} \tag{8}$$

in this context, t_n, t_s, and t_t represent the normal stress and the two mutually perpendicular shear stresses, respectively, while δ_s, δ_n, and δ_t correspond to the relative normal displacement and the two perpendicular relative shear displacements. k_{nn}, k_{ss}, and k_{tt} are the components of the stiffness matrix. If only the stiffness of the mortar is considered in the modeling, the components of the stiffness matrix are solely functions of the mortar's stiffness and dimensions. However, since the simplified masonry micro-model is used in this study, the stiffness of the expanded bricks also affects the components of this stiffness matrix.

So, the equivalent stiffness for joint interfaces is expressed as a function of the mortars and unit's moduli of elasticity, and the thickness of the mortar.

$$k_{nn} = \frac{E_u E_m}{h_m(E_u - E_m)} \tag{9}$$

$$k_{ss} = k_{tt} = \frac{G_u G_m}{h_m(G_u - G_m)} \tag{10}$$

where h_m is the thickness of the mortar, and E_u and E_m are the Young's moduli of the masonry unit and the mortar, respectively. Similarly, G_u and G_m represent the shear moduli of the masonry unit and the mortar, respectively. The initial linear response of the joints is followed by crack propagation. When the damage initiation criterion is achieved based on the user-defined tractions between the masonry interfaces, i.e., shear and tensile strength of the joints, cracking propagates in the masonry joints.

The damage initiation criterion can be defined based on either separation or stress, each of which includes two types of damage initiation criteria. In this study, the stress-based criterion is used for damage initiation. The stress criterion includes the Maximum Stress Criterion and the Quadratic Stress Criterion. These two damage initiation criteria are presented in Eqs. 11 and 12, respectively.

$$max\left\{\frac{t_n}{t_n^0}, \frac{t_t}{t_t^0}, \frac{t_s}{t_s^0}\right\} = 1 \tag{11}$$

$$\left[\frac{t_n}{t_n^0}\right]^2 + \left[\frac{t_t}{t_t^0}\right]^2 + \left[\frac{t_s}{t_s^0}\right]^2 = 1 \tag{12}$$

in these equations, t_n^0, t_t^0, and t_s^0 represent the maximum normal stress and the two orthogonal shear stresses, respectively. In both criteria, t_n is always considered positive, since compressive stress cannot cause cracking in the joint interface. These two criteria are represented in Fig. 8. In this study, the Quadratic Stress Criterion is used for damage initiation.

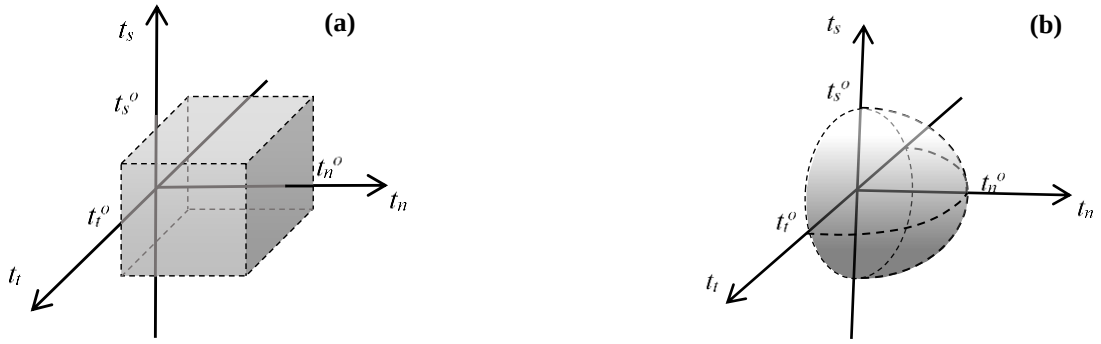

Fig. 8. Criterion for the onset of nonlinear behavior of mortar: (a) cubic, and (b) quadratic.

After reaching the maximum stress in shear and tension, the nonlinear behavior exhibits softening. This softening behavior is defined in the software using an exponential function. In this range, damage (cracking) propagates within the interface, leading to a reduction in stiffness. This stiffness degradation is incorporated into the constitutive equation according to the following relation.

$$\begin{bmatrix} t_n \\ t_s \\ t_t \end{bmatrix} = (1 - D) \begin{bmatrix} k_{nn} & 0 & 0 \\ 0 & k_{ss} & 0 \\ 0 & 0 & k_{tt} \end{bmatrix} \begin{bmatrix} \delta_n \\ \delta_s \\ \delta_t \end{bmatrix} \tag{13}$$

in the above equation, D is the damage variable, with a value ranging between 0 and 1. A value of 0 indicates no damage in the interface, while a value of 1 signifies that the interface is fully damaged and can no longer transfer shear or tensile stresses.

5. Numerical model

Based on the information presented in the previous sections, the simplified micro-model consists of two main components. The first component is the expanded masonry units. These units are larger than their actual size by the thickness of the mortar. Since the

masonry units are modeled in three dimensions, solid elements with 8 nodes and reduced integration (C3D8R) were used to simulate their behavior, with dimensions of 30 × 30 × 33 mm. The mechanical properties of the masonry unit are provided in Table 1.

Table 1. Mechanical specifications of the expanded masonry unit.

Linear behavior			Nonlinear behavior	
Elastic modulus of units (MPa)	**Poisson's ratio**	**Adjusted elastic modulus of the expanded unit (MPa)**	**Tensile strength (MPa)**	**Compressive strength (MPa)**
16700	0.15	4050	2	15

To define the interaction between the masonry elements, four parameters were used: tangential behavior, normal behavior, cohesive behavior, and damage. When surfaces come into contact, they typically transmit both shear and normal forces across their interface. A relationship usually exists between these two force components. This relationship, referred to as tangential behavior between the contacting bodies, is commonly described in terms of the stresses at the interface. The friction coefficient for the tangential behavior was assumed to be 0.75.

The distance between two surfaces is referred to as the clearance. In Abaqus, the contact constraint is enforced when the clearance between the two surfaces becomes zero. There is no limit in the contact formulation regarding the magnitude of contact pressure that can be transmitted between the surfaces. The surfaces separate when the contact pressure becomes zero or negative, at which point the constraint is removed. This type of normal behavior, known as hard contact, is used to define the contact interaction. The Cohesive behavior and Damage parameters represent the linear and nonlinear behavior of the mortar. The detailed specifications of these parameters are provided in Table 2.

Table 2. Mechanical specifications of the mortar.

Linear behavior				Nonlinear behavior			
Elastic modulus of mortar (MPa)	**K_{nn} (N/mm^3)**	**K_{ss} (N/mm^3)**	**K_{tt} (N/mm^3)**	**Maximum tensile stress (MPa)**	**G_{IC} (N/mm)**	**Cohesion (MPa)**	**G_{IIC} (N/mm)**
780	82	36	36	0.25	0.18	0.35	0.125

In Fig. 9, the numerical model is shown. As illustrated in the figure, to apply boundary conditions, the bottom of the wall footing is fully restrained in all three orthogonal directions. A distributed load of 0.3 MPa is applied to the top of the beam, and a lateral load is applied to the top of the beam using a displacement-controlled approach. To validate the model, two parameters are compared with the experimental results: base shear and failure mode.

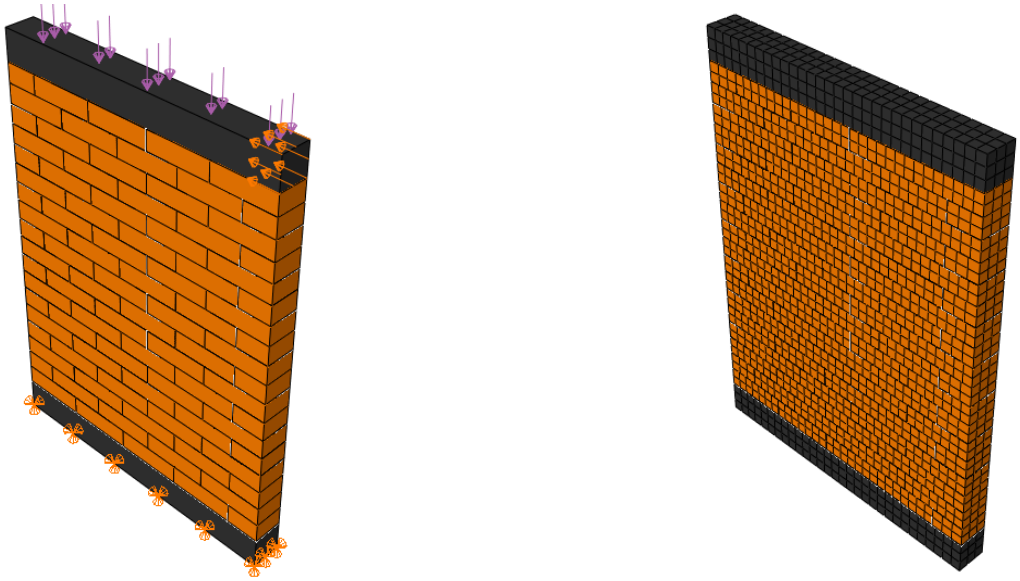

Fig. 9. Numerical model with meshing and boundary conditions.

Fig. 10 presents the base shear diagram under monotonic loading, which demonstrates a reasonable agreement between the numerical and experimental models. This figure also shows the failure modes of the numerical and experimental masonry walls. As illustrated, the failure mode in both cases is shear-diagonal, indicating that the numerical wall successfully replicates the behavior observed in the experimental model.

To investigate sensitivity, the numerical wall was modeled using meshes of various sizes: 20, 30, 40, and 50 mm. Fig. 11 presents the base shear diagrams corresponding to the different mesh sizes. As seen in the figure, smaller mesh sizes result in more converged base shear responses. Since the wall modeled with a 30 mm mesh provides a good balance between computational efficiency and accuracy, this mesh size was chosen for the final modeling of the wall.

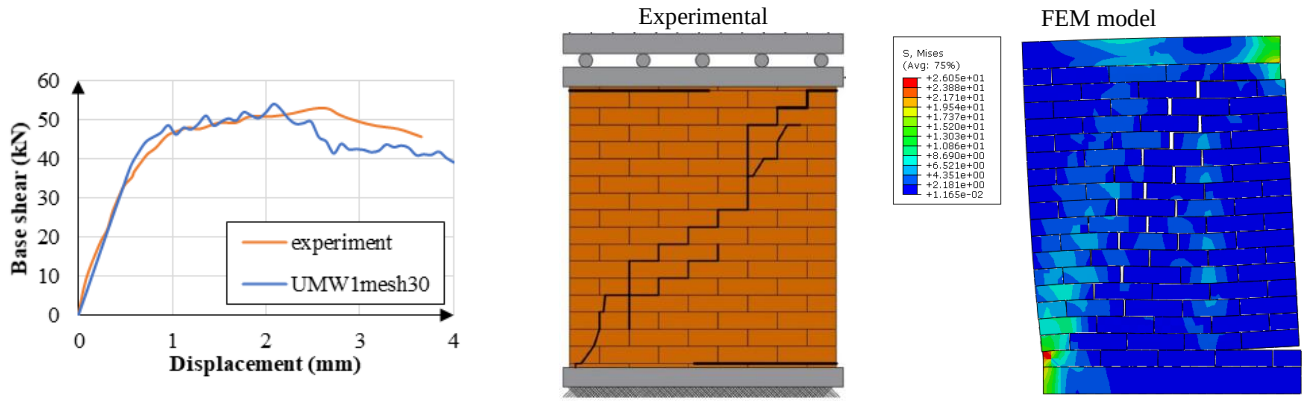

Fig. 10. Base shear diagram and the failure mode.

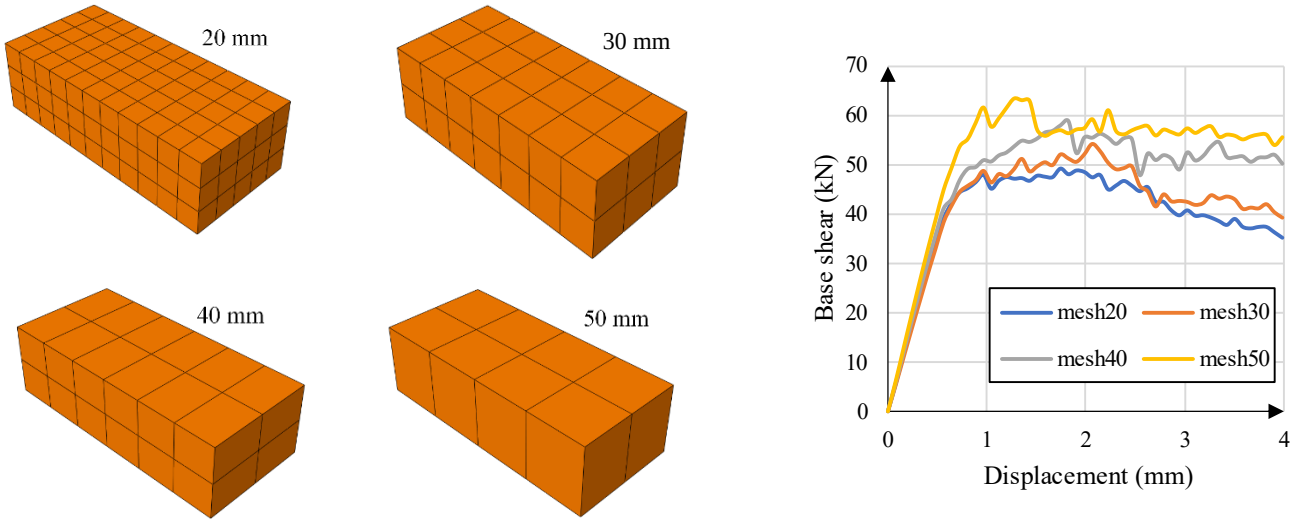

Fig. 11. Sensitivity of the numerical model based on different mesh dimensions.

In this study, Fe-SMA strips were used to investigate the effect of post-tensioning on masonry walls. These strips are made of Fe-SMA with 1.5 mm thickness and a width of 120 mm. The modulus of elasticity and yield stress in this type of alloy are 165 GPa and 400 MPa, respectively, and the austenite onset temperature is approximately 180 degrees Celsius. This type of Fe-based alloy must be heated to 160 °C to create post-tension stress. Because these materials are highly electrically resistant, the alloy's temperature can be easily increased as needed by the electric current. In the numerical modeling of SMA strips, shell elements are used. These elements are of the 4-node type, and tie interaction is used to connect them to the wall body. With this method, the modeling level is less complex and the model faces fewer errors analytically.

6. Results of numerical models

In this study, three numerical models were developed to improve the behavior of the masonry wall. The first model, as shown in Fig. 12a, utilized vertical strips to strengthen the wall. The second and third models, depicted in Fig. 12, employed SMA strips in V-shaped and Λ-shaped configurations, respectively.

Since the level of post-tensioning stress in iron-based alloys can vary depending on boundary and operational conditions, this research considered post-tensioning stress levels of 100 MPa, 200 MPa, 300 MPa, and 400 MPa to analyze their effects on the masonry wall. The models were subjected to monotonic lateral loads. The primary aim was to evaluate how different reinforcement strategies and post-tensioning stress levels impact the structural response of the wall under lateral loading. The results obtained from these three models were then compared to each other to determine the most effective reinforcement method for enhancing the stability and ductility of the masonry wall.

This comparative analysis provides valuable insights into the behavior of reinforced walls under seismic or other lateral forces, helping structural engineers optimize design strategies for safer, more resilient buildings. The use of SMA strips can significantly enhance the behavior and lateral resistance of masonry walls. This study evaluates the lateral strength of masonry walls reinforced with SMA strips, comparing them to conventional walls. Fig. 13 presents the resistance of these reinforced walls, illustrating the influence of the post-tensioning on their structural response. To facilitate analysis, the post-tensioned masonry walls are designated by the notation MW-Ve300, where "MW" stands for Masonry Wall, "Ve" indicates a vertical (perpendicular) orientation, and "300" reflects the level of post-tensioning stress in megapascals. The results demonstrate that as the degree of post-tensioning increases, the lateral resistance of the wall also increases. Consequently, all post-tensioned masonry walls exhibit higher lateral resistance

compared to normal, non-post-tensioned walls. This phenomenon is primarily attributed to the coefficient of friction, which plays a crucial role in converting the applied vertical (post-tensioning) forces into lateral resistance. When the post-tensioning load acts vertically on the wall, this load is effectively transformed into lateral resistance via the frictional interaction between the masonry components and the SMA strips.

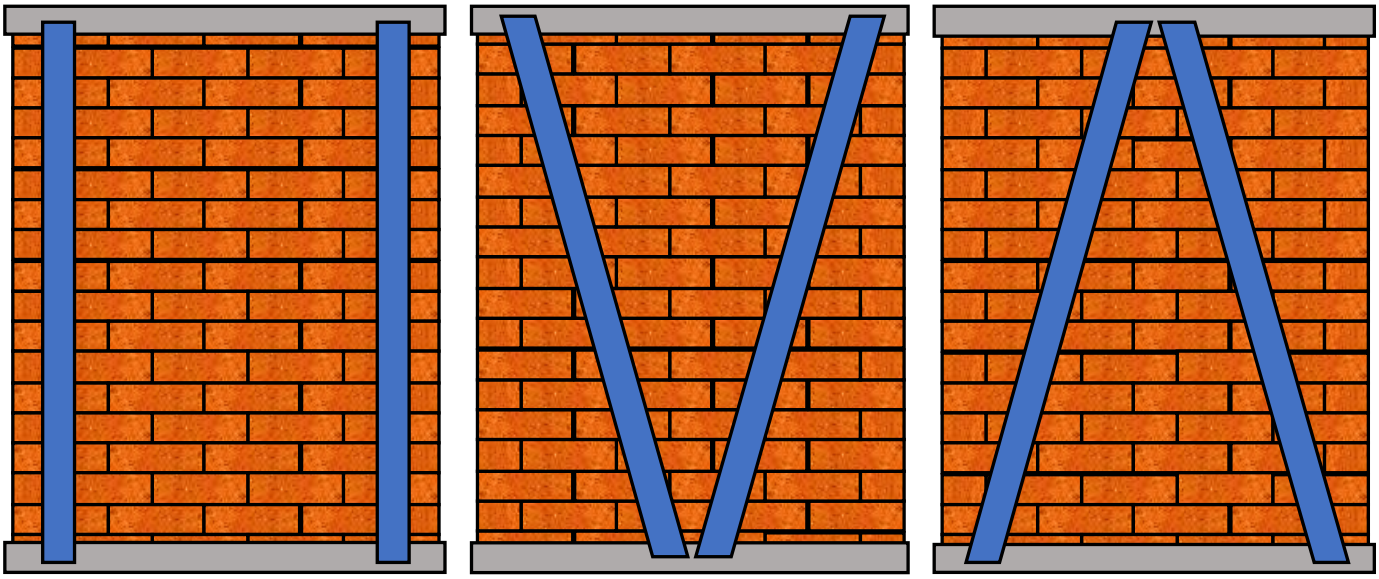

Fig. 12. Models reinforced with SMA strips: (a) Vertical, (b) V-shaped, and (c) Λ-shaped.

Specifically, as the level of post-tensioning stress increases, the coefficient of friction enhances, leading to a corresponding rise in the wall's lateral resistance. The measured lateral resistances for the MW-Ve100, MW-Ve200, MW-Ve300, and MW-Ve400 walls are 59.3, 68.1, 78.1, and 95.5 Newtons, respectively. These figures indicate that the lateral resistance of these walls improves by approximately 22%, 40%, 61%, and 96% compared to a baseline masonry wall without reinforcement. A key observation in this investigation is that the increase in resistance is not directly caused by the SMA strips themselves but is mediated through their effect on the frictional interaction. The SMA strips indirectly contribute to enhancing the resistance by increasing the effective coefficient of friction at the interface, thus facilitating the conversion of vertical post-tensioning into effective lateral resistance.

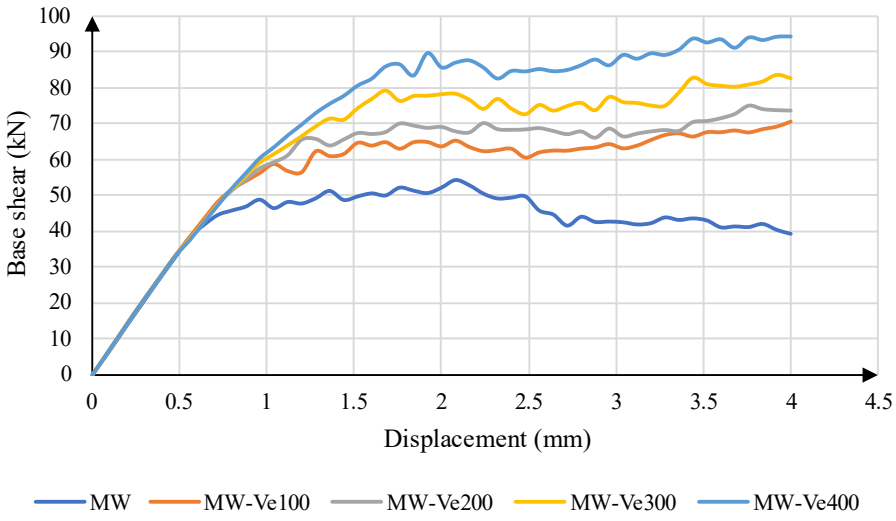

Fig. 13. Base shear of masonry walls reinforced with vertical strips.

Fig. 14 illustrates the base shear diagram for reinforced masonry walls with a V-shaped configuration. As depicted in the figure, the utilization of Shape Memory Alloy (SMA) strips has significantly enhanced the lateral resistance of the structural wall. Furthermore, the increase in applied post-tension within these SMA strips correlates with a corresponding rise in the wall's lateral resistance, indicating that higher post-tensioning levels contribute positively to the overall seismic performance of the structure. For analytical clarity, the post-tensioned masonry walls are designated by the notation MW-V300, where "MW" refers to Masonry Wall, "V" signifies the V-shaped reinforcement configuration, and "300" indicates the level of post-tensioning stress expressed in megapascals (MPa). An important observation derived from this figure is that two primary factors influence the enhancement of the wall's lateral resistance. First, in the case of purely vertical post-tensioning, the coefficient of friction between masonry units predominantly governs the resistance increase. Conversely, in the V-shaped wall configuration, beyond the frictional interactions between masonry units, the SMA alloys directly contribute to the lateral load resistance. It should be noted that these SMA strips are inclined rather than vertical; thus, they exert less vertical post-tensioning force compared to vertically reinforced walls. As a

result, the frictional contribution to lateral resistance in the V-shaped walls is relatively less significant. Nonetheless, due to the inclined orientation of the SMA strips, they can function similarly to braces, actively enhancing the overall stiffness and strength of the masonry wall against lateral loads. Experimental assessments of the lateral resistance capacities for the walls designated MW-V100, MW-V200, MW-V300, and MW-V400 are 57.3 N, 63.1 N, 70.2 N, and 77.5 N, respectively. These measurements demonstrate that the lateral resistance increases by approximately 14%, 26%, 40%, and 55%, respectively, compared to a baseline unreinforced masonry wall, highlighting the substantial beneficial effect of SMA reinforcement. Furthermore, the stiffness evaluation depicted in the figure indicates that models equipped with SMA reinforcement exhibit higher stiffness values than conventional walls. This improvement is primarily attributable to the inclined orientation of the SMA strips, which enhances the structural integrity and resilience of the masonry walls under lateral seismic forces.

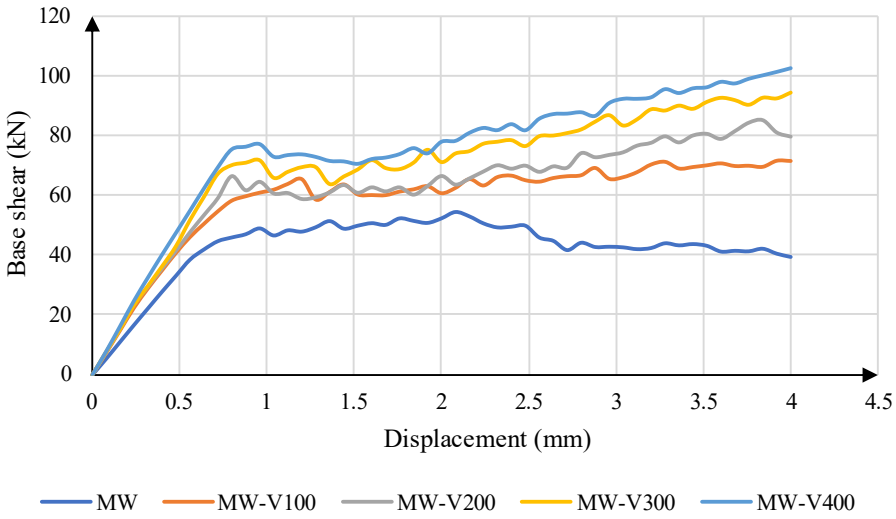

Fig. 14. Base shear of masonry walls reinforced with V-shaped strips.

Fig. 15 presents the base shear diagram for reinforced masonry walls with a Λ-shaped configuration. As shown in the figure, these SMA strips result in a corresponding enhancement of the wall's lateral capacity. This indicates that increasing the post-tension level directly contributes to improved seismic resistance, making the walls more capable of withstanding dynamic lateral loads. To facilitate a standardized analysis, the post-tensioned masonry walls are designated by the notation MW-Λ300, where "MW" signifies Masonry Wall, "Λ" indicates the Λ-shaped reinforcement configuration, and "300" denotes the level of post-tensioning stress, measured in megapascals (MPa).

A noteworthy aspect of this diagram is that two primary factors influence the enhancement of the wall's lateral resistance. First, in the case of purely vertical post-tensioning, the coefficient of friction between masonry units is predominantly responsible for increasing the resistance. However, in the Λ-shaped reinforced walls, in addition to the frictional interaction between masonry units, the SMA alloys play a direct role in resisting lateral forces. It is important to note that these SMA strips are installed in an inclined (non-vertical) orientation; thus, they exert less vertical post-tensioning force compared to purely vertical reinforcement. Consequently, the contribution of friction to the overall lateral resistance in Λ-shaped walls is comparatively reduced. Nonetheless, due to their inclined orientation, these SMA strips can act similarly to braces, actively contributing to the overall stiffness and strength of the masonry structure during seismic events. Experimental measurements of the lateral resistance for the walls designated as MW-Λ100, MW-Λ200, MW-Λ300, and MW-Λ400 are 62.4 N, 66.8 N, 73.2 N, and 80.5 N, respectively. These results demonstrate that the lateral resistance increases progressively by approximately 24%, 33%, 46%, and 61%, respectively, compared to a baseline masonry wall without reinforcement. This significant improvement underscores the effectiveness of incorporating SMA-based reinforcement strategies in enhancing seismic resilience. Furthermore, the data shown in the figure indicate that the stiffness of the models equipped with SMA reinforcement exceeds that of standard, unreinforced masonry walls. This increase in stiffness is primarily attributable to the inclined orientation of the SMA strips, which effectively enhances the structural integrity and load-bearing capacity of the walls under lateral seismic forces. Overall, the incorporation of inclined SMA strips in masonry walls demonstrates a promising approach for strengthening seismic performance.

Fig. 16 presents a schematic illustration of the failure mode of the masonry wall. Given that the failure mode of a typical unreinforced masonry wall predominantly occurs along a diagonal crack, the increase in vertical stress levels does not significantly alter the fundamental mode of failure. Instead, the failure mode remains primarily characterized by diagonal behavior along a diagonal plane, which is typical for such structural configurations. This observation indicates that, despite variations in prestressing, the mode of failure remains consistent, highlighting the inherent diagonal nature of conventional masonry walls under lateral loading conditions.

7. Conclusion

In this study, Fe-based Shape Memory Alloys (Fe-SMAs) were utilized as a strengthening material to improve the behavior of masonry walls subjected to lateral loading. The numerical models, validated against experimental data, demonstrated that Fe-SMA

strips significantly enhance the lateral resistance, stiffness, and ductility of masonry walls. These alloys, which possess the unique ability to return to their original shape upon heating, enable the application of post-tensioning forces both vertically and diagonally. This property is particularly valuable for seismic strengthening of unreinforced masonry structures.

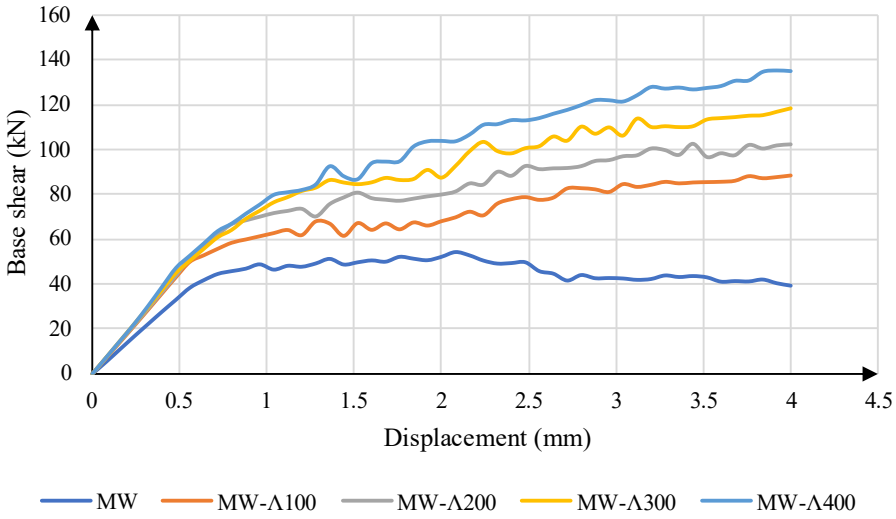

Fig. 15. Base shear of masonry walls reinforced with Λ-shaped strips.

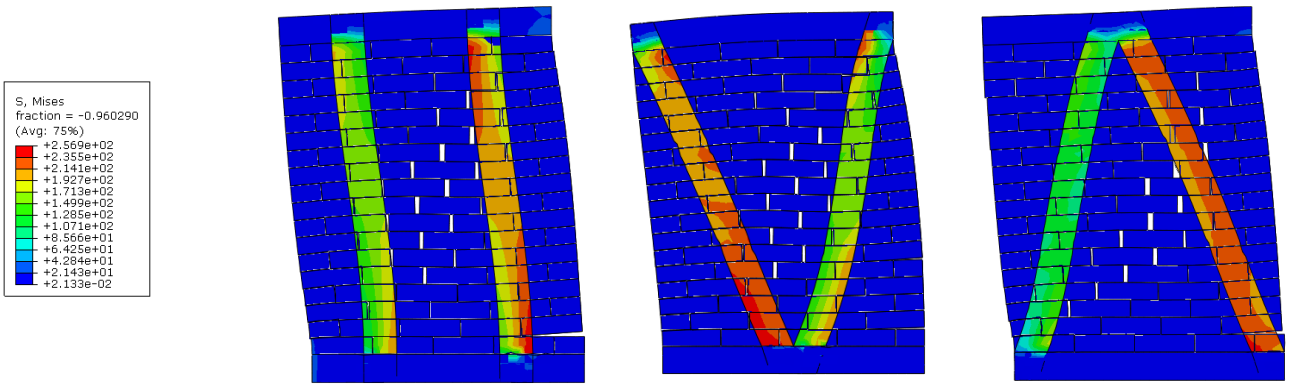

Fig. 16. Failure mode of reinforced masonry walls.

These findings have significant practical implications for structural engineers involved in the seismic retrofitting of unreinforced masonry (URM) buildings. The demonstrated effectiveness of Fe-SMA strips in enhancing lateral strength and ductility offers a viable solution for upgrading existing masonry walls, particularly in earthquake-prone regions. Due to their thermal activation mechanism, Fe-SMAs enable easy application of post-tensioning without requiring mechanical anchorage systems, which simplifies installation and minimizes intervention in heritage or occupied structures. Moreover, the ability to configure reinforcement in vertical and diagonal patterns provides design flexibility based on architectural constraints and desired performance levels. Engineers can integrate this technique into performance-based retrofit strategies, using numerical modeling tools like Abaqus to predict behavior and optimize reinforcement layout and post-tensioning levels before implementation. As such, Fe-SMA-based retrofitting can serve as a practical and cost-effective approach in both emergency strengthening scenarios and long-term rehabilitation programs.

It is important to note that in the current study, the Fe-SMA strips were modeled using fixed mechanical properties corresponding to their post-activation state. However, Fe-SMAs exhibit temperature-dependent behavior, particularly during thermal activation, where phase transformation from martensite to austenite occurs and influences stress development. While this simplification does not significantly affect the global structural response after activation, it may limit the accuracy in capturing transient thermal-mechanical interactions. Future studies are encouraged to adopt coupled thermo-mechanical models or user-defined material subroutines to simulate the evolution of recovery stress during activation and cooling phases for a more comprehensive analysis.

1. Three reinforcement configurations were evaluated: vertically oriented strips, V-shaped, and Λ-shaped arrangements. Post-tensioning stress levels of 100 MPa, 200 MPa, 300 MPa, and 400 MPa were applied to assess their influence on structural performance. The results showed a clear trend: as the level of post-tensioning increased, so did the lateral resistance of the wall. In the vertically reinforced walls, the improvement was primarily due to the frictional forces enhanced by the vertical post-tensioning. Conversely, in the V- and Λ-shaped configurations, in addition to frictional improvement, the SMA strips acted as diagonal braces, directly contributing to the lateral stiffness and resistance.
2. Vertically reinforced walls exhibited up to 96% improvement in lateral resistance compared to the unreinforced wall. V-

shaped and Λ-shaped reinforcements showed increases of approximately 55% and 61%, respectively. Furthermore, the stiffness of the walls improved significantly in all reinforced models, particularly in the inclined configurations due to their bracing effect, which helped in resisting lateral deformation more effectively.

3. Importantly, the mode of failure in all cases remained primarily diagonal shear, which is typical for masonry walls under lateral loading. This indicates that while the post-tensioning improved the performance characteristics, such as strength and stiffness, it did not alter the fundamental failure mechanism. Instead, it delayed the onset of failure and enhanced energy dissipation.

In conclusion, Fe-SMA strips offer a promising, cost-effective, and easily implementable solution for strengthening masonry walls. Their ability to generate post-tensioning forces through thermal activation allows for innovative reinforcement strategies in both vertical and diagonal directions. The findings of this study suggest that Fe-SMAs can be a highly effective tool in seismic retrofitting, enhancing the resilience and safety of masonry structures in earthquake-prone regions. This approach not only improves structural performance but also provides a practical pathway for future research and real-world applications in earthquake engineering.

8. Limitations

While the findings of this study provide valuable insights into the application of Fe-based Shape Memory Alloys (Fe-SMAs) for seismic strengthening of masonry walls, several limitations should be acknowledged. First, the numerical analysis was conducted using the Simplified Micro-modeling approach, which assumes homogenized interaction properties and does not capture detailed micro-cracking or localized stress concentrations at the brick–mortar interface. Second, the study focused solely on monotonic in-plane loading, whereas cyclic or dynamic loading—more representative of real seismic events—was not considered. This may limit the assessment of energy dissipation and degradation behavior. Third, boundary conditions in the model were idealized (e.g., fully fixed base and uniformly distributed vertical load), which may not fully reflect real-world constraints or irregular support conditions in existing buildings. Additionally, the bonding between Fe-SMA strips and masonry was modeled as perfectly rigid, neglecting potential issues such as debonding or interface slip. Future research incorporating more detailed material interfaces, experimental validation under cyclic loads, and practical field-scale testing will be essential to generalize the applicability of the proposed method.

Statements & Declarations

Author contributions

Moein Rezapour: Investigation, Formal analysis, Validation, Resources, Writing - Original Draft, Writing - Review & Editing.

Mehdi Ghassemieh: Conceptualization, Methodology, Project administration, Supervision, Writing - Review & Editing.

Funding

The authors received no financial support for the research, authorship, and/or publication of this article.

Data availability

The data presented in this study will be available on interested request from the corresponding author.

Declarations

The authors declare no conflict of interes.

References

[1] Maheri, M., Najafgholipour, M., Rajabi, A. The influence of mortar head joints on the in-plane and out-of-plane seismic strength of brick masonry walls. Iranian Journal of Science and Technology, 2011; 35: 63-79. doi:10.22099/ijstc.2012.657.

[2] Nateghi, F., Alemi, F. Experimental study of seismic behaviour of typical Iranian URM brick walls. In: 14th World Conference on Earthquake Engineering; 2008 Oct 12-17; Beijing, China. p. 123-130.

[3] Griffith, M. C., Vaculik, J., Lam, N., Wilson, J., Lumantarna, E. Cyclic testing of unreinforced masonry walls in two-way bending. Earthquake Engineering & Structural Dynamics, 2007; 36: 801-821. doi:10.1002/eqe.654.

[4] ElGawady, M., Lestuzzi, P., Badoux, M. Performance of URM walls under in-plane seismic loading. The Masonry Society Journal, 2005; 23: 85-104. doi:10.70803/001c.138950.

[5] Gouveia, J. P., Lourenço, P. B. Masonry shear walls subjected to cyclic loading: influence of confinement and horizontal reinforcement. In: North American Masonry Conference; 2007 June 3-6; St. Louis, Missouri. p. 838–848.

[6] Petry, S., Beyer, K. Cyclic test data of six unreinforced masonry walls with different boundary conditions. Earthquake Spectra, 2015; 31: 2459-2484. doi:10.1193/101513EQS269.

[7] Wang, Q., Shi, Q., Tao, Y. Seismic behavior and shear strength of new-type fired perforated brick walls with high void ratio. Advances in Structural Engineering, 2019; 22: 1035-1048. doi:10.1177/1369433218802690.

[8] ElGawady, M. A., Lestuzzi, P., Badoux, M. Aseismic retrofitting of unreinforced masonry walls using FRP. Composites Part B: Engineering, 2005; 37: 148-162. doi:10.1016/j.compositesb.2005.06.003.

[9] Shabdin, M., Khajeh Ahmad Attari, N., Zargaran, M. Experimental Study on Seismic Behavior of Unreinforced Masonry (URM) Brick Walls Strengthened in the Boundaries with Shotcrete. Journal of Earthquake Engineering, 2019; 1-27. doi:10.1080/13632469.2019.1577763.

[10] Hamakareem, M. I. Prestressed Masonry -Methods of Prestressing, Advantages and Applications. 2025. https://theconstructor.org/concrete/prestressed-masonry-methods-advantages-applications/16173/.

[11] Sadeghi Marzaleh, A. Seismic in-plane behavior of post-tensioned existing clay brick masonry walls, (PhD Thesis). Zurich (CH): University of ETH Zurich; 2015.

[12] Schultz, A. E., Scolforo, M. J. Overview of prestressed masonry. The Masonry Society Journal, 1991; 10: 6-21. doi:10.70803/001c.141160.

[13] Kohail, M., Elshafie, H., Rashad, A., Okail, H. Behavior of post-tensioned dry-stack interlocking masonry shear walls under cyclic in-plane loading. Construction and Building Materials, 2019; 196: 539-554. doi:10.1016/j.conbuildmat.2018.11.149.

[14] Soltanzadeh, G., Osman, H. B., Vafaei, M., Vahed, Y. K. Seismic retrofit of masonry wall infilled RC frames through external post-tensioning. Bulletin of Earthquake Engineering, 2018; 16: 1487-1510. doi:10.1007/s10518-017-0241-4.

[15] Hassanli, R. Simplified approach to predict the flexural strength of unbonded post-tensioned masonry walls. 1st ed. Cham: Springer; 2019. doi:10.1007/978-3-319-93788-5_6.

[16] Hassanli, R. Flexural Strength Prediction of Unbonded Post-tensioned Masonry Walls. 1st ed. Cham: Springer; 2018. doi:10.1007/978-3-319-93788-5_5.

[17] Hassanli, R. Experimental Investigation of Unbonded Post-tensioned Masonry Walls. 1st ed. Cham: Springer; 2019. doi:10.1007/978-3-319-93788-5_7.

[18] Hassanli, R. Strength and Seismic Performance Factors of Post-tensioned Masonry Walls. 1st ed. Cham: Springer; 2018. doi:10.1007/978-3-319-93788-5_3.

[19] Laursen, P. T., Ingham, J. M. Structural testing of single-storey post-tensioned concrete masonry walls. The Masonry Society Journal, 2001; 19: 69-82. doi:10.70803/001c.142720.

[20] Quiroz, A. P. Seismic vulnerability of historic masonry towers by external prestressing devices, (PhD Thesis). University of Naples Federico; 2011.

[21] Babatunde, S. A. Review of strengthening techniques for masonry using fiber reinforced polymers. Composite Structures, 2017; 161: 246-255. doi:10.1016/j.compstruct.2016.10.132.

[22] Seim, W., Pfeiffer, U. Local post-strengthening of masonry structures with fiber-reinforced polymers (FRPs). Construction and Building Materials, 2011; 25: 3393-3403. doi:10.1016/j.conbuildmat.2011.03.030.

[23] Hong, K.-N., Yeon, Y.-M., Shim, W.-B., Kim, D.-H. Recovery Behavior of Fe-Based Shape Memory Alloys under Different Restraints. Applied Sciences, 2020; 10: 3441. doi:10.3390/app10103441.

[24] Choi, E., Ostadrahimi, A., Kim, W. J., Seo, J. Prestressing effect of embedded Fe-based SMA wire on the flexural behavior of mortar beams. Engineering Structures, 2021; 227: 111472. doi:10.1016/j.engstruct.2020.111472.

[25] Shahverdi, M., Michels, J., Czaderski, C., Motavalli, M. Iron-based shape memory alloy strips for strengthening RC members: Material behavior and characterization. Construction and Building Materials, 2018; 173: 586-599. doi:10.1016/j.conbuildmat.2018.04.057.

[26] Shahverdi, M., Czaderski, C., Motavalli, M. Iron-based shape memory alloys for prestressed near-surface mounted strengthening of reinforced concrete beams. Construction and Building Materials, 2016; 112: 28-38. doi:10.1016/j.conbuildmat.2016.02.174.

[27] Shahverdi, M., Czaderski, C., Annen, P., Motavalli, M. Strengthening of RC beams by iron-based shape memory alloy bars embedded in a shotcrete layer. Engineering Structures, 2016; 117: 263-273. doi:10.1016/j.engstruct.2016.03.023.

[28] Izadi, M., Motavalli, M., Ghafoori, E. Iron-based shape memory alloy (Fe-SMA) for fatigue strengthening of cracked steel bridge connections. Construction and Building Materials, 2019; 227: 116800. doi:10.1016/j.conbuildmat.2019.116800.

[29] Izadi, M., Ghafoori, E., Shahverdi, M., Motavalli, M., Maalek, S. Development of an iron-based shape memory alloy (Fe-SMA) strengthening system for steel plates. Engineering Structures, 2018; 174: 433-446. doi:10.1016/j.engstruct.2018.07.073.

[30] Izadi, M., Ghafoori, E., Motavalli, M., Maalek, S. Iron-based shape memory alloy for the fatigue strengthening of cracked steel plates: Effects of re-activations and loading frequencies. Engineering Structures, 2018; 176: 953-967. doi:10.1016/j.engstruct.2018.09.021.

[31] Izadi, M., Ghafoori, E., Hosseini, A., Motavalli, M., Maalek, S., Shahverdi, M. Feasibility of iron-based shape memory alloy strips for prestressed strengthening of steel plates. In: The fourth International Conference on Smart Monitoring, Assessment and Rehabilitation of Civil Structures (SMAR 2017); 2017 Sep 13-15; Zurich, Switzerland. p. 260-268.

[32] Rezapour, M., Ghassemieh, M., Motavalli, M., Shahverdi, M. Numerical Modeling of Unreinforced Masonry Walls Strengthened with Fe-Based Shape Memory Alloy Strips. Materials, 2021; 14: 2961. doi:10.3390/ma14112961.

[33] Lagoudas, D. C. Shape memory alloys: modeling and engineering applications. 1st ed. New York (NY): Springer; 2008. doi:10.1007/978-0-387-47685-8.

[34] Vermeltfoort, A. T., Raijmakers, T., Janssen, H. Shear tests on masonry walls. In: 6th North American Masonry Conference; 1993 Jun 6-9; Philadelphia, Pennsylvania. p. 1183-1193.

[35] Lourenço, P. J. B. B. Computational strategies for masonry structures, (PhD Thesis). Delft (NL): Delft university Press; 1996.

[36] Rezapour, M., Ghassemieh, M. Macroscopic modelling of coupled concrete shear wall. Engineering Structures, 2018; 169: 37-54. doi:10.1016/j.engstruct.2018.04.088.

[37] Lee, J., Fenves, G. L. Plastic-damage model for cyclic loading of concrete structures. Journal of Engineering Mechanics, 1998; 124: 892-900. doi:10.1061/(ASCE)0733-9399(1998)124:8(892).

[38] Lubliner, J., Oliver, J., Oller, S., Oñate, E. A plastic-damage model for concrete. International Journal of Solids and Structures, 1989; doi:10.1016/0020-7683(89)90050-4.

[39] Mander, J. B., Priestley, M. J., Park, R. Theoretical stress-strain model for confined concrete. Journal of Structural Engineering, 1988; 114: 1804-1826. doi:10.1061/(ASCE)0733-9445(1988)114:8(1804).

[40] Selby, R. G., Vecchio, F. J. A constitutive model for analysis of reinforced concrete solids. Canadian Journal of Civil Engineering, 1997; 24: 460-470. doi:10.1139/l96-135.